Supplemental information

Cobalt-modified covalent organic framework enables highly efficient degradation of 2,4-dichlorophenol in high concentrations through peroxymonosulfate activation

Yunchao Ma[a], Yuhang Han[a], Yuxin Yao[a], Tianyu Zhou[a,b], Dongshu Sun[a], Chunbo Liu[b,*] Guangbo Che[c,*], Bo Hu [a,*] Valentin Valtchev[d] and Qianrong Fang[e]

[a]*Key Laboratory of Preparation and Application of Environmental Friendly Materials (Jilin Normal University), Ministry of Education, Changchun, 130103, P.R. China*

[b]*Jilin Joint Technology Innovation Laboratory of Developing and Utilizing Materials of Reducing Pollution and Carbon Emissions, College of Engineering, Jilin Normal University, Siping, 136000, China*

[c]*College of Chemistry, Baicheng Normal University, Baicheng, 137000, China*

[d]*Qindao Institute of Bioenergy and Bioprocess Technology Chinese Academy of Sciences, 189 Song Ling Rd, Qingdao, Shangdong 266101, China.*

[e]*State Key Laboratory of Inorganic Synthesis and Preparative Chemistry, Jilin University, Changchun 130012, China*

Table of contents

Section S1. Materials and characterization

S1.1 Materials and instruments

All starting materials and solvents, unless otherwise noted, were obtained from J&K scientific LTD. 2,4,6-tri(4-aldehyde phenyl)-1,3,5-triazine (TFPT) was purchased from J&K scientific LTD. 2,2'-bipyridine-5,5'-diamine (Bpy) was purchased from Zhengzhou Alpha Chemical Technology Co.. Fourier transform infrared (FT-IR) spectra were acquired on a Thermoscientific Nicolet 4700 Fourier Transform Infrared Spectrometer with KBr pellet. Thermogravimetric analysis (TGA) was recorded on a STA 449 F3 Jupiter thermal analyzer with N_2 flow rate of 20 mL min^{-1} at a heating rate of 5 ℃ min^{-1} to 800 ℃. PXRD data were collected on a PANalytical B.V. Empyrean powder diffractometer using a Cu Kα source (λ = 1.5418 Å) over the range of 2θ = 2.0-40.0° with a step size of 0.02° and 2 s per step. The SEM images were obtained on JEOL 8100 scanning electron microscope. X-ray photoelectron spectroscopy (XPS) and UV-vis diffuse reflectance spectrum (UV-vis DRS) and UV detection were obtained by ESCALAB250XI electronic spectrometer (VG scientific, USA).

S1.2 Synthesis of JLUN-307

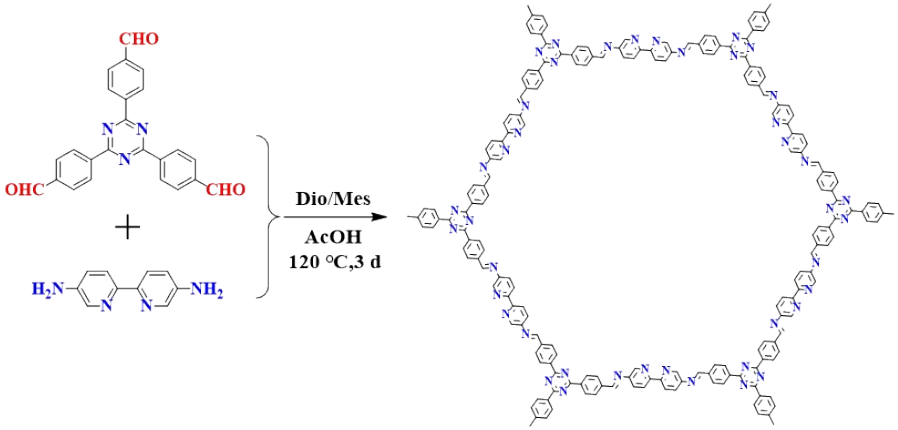

TFPT (0.04 mmol, 15.73 mg) and Bpy (0.06 mmol, 11.17 mg) were weighed into a Pyrex tube (volume: ca. 20 mL with length of 10 cm, neck length of 9 cm) and to the mixture were added 1,4-dioxane (0.5 mL), 1,3,5-trityleneand (0.5 mL) and 0.1 mL of aqueous acetic acid (6.0 mol L^{-1}). The tube was flash frozen at 77K (LN_2 bath), evacuated to an internal pressure of 0.15 mmHg and flame sealed. Upon sealing, the length of the tube was reduced to ca. 13 cm. The reaction mixture was heated at 120℃ for 72 h to afford a yellow precipitate which was isolated by filtration over a medium glass frit and washed with anhydrous acetone (3×20 mL). The yield was about 82.1% (22.1 mg). The solvent was removed under vacuum at 60 ℃ to afford the corresponding products as yellow powder of JLNU-307 (JLNU=Jilin Normal University). Anal. Calc for $C_{78}H_{48}N_{18}$: C: 77.16; H: 3.65; N:19.19 Found: C:77.91; H:

3.52; N: 18.57. Solid-state ^{13}C NMR (500MH_Z): 74.14, 88.79, 93.83, 121.63, 128.68, 139.15, 145.28, 153.79, 158.29, 170.38 ppm. FT-IR (KBr): 805, 1031, 1189, 1345, 1376, 1407, 1496, 1602, 1679, 2913, 3417 cm^{-1}.

S1.3 Synthesis of JLUN-307-Co

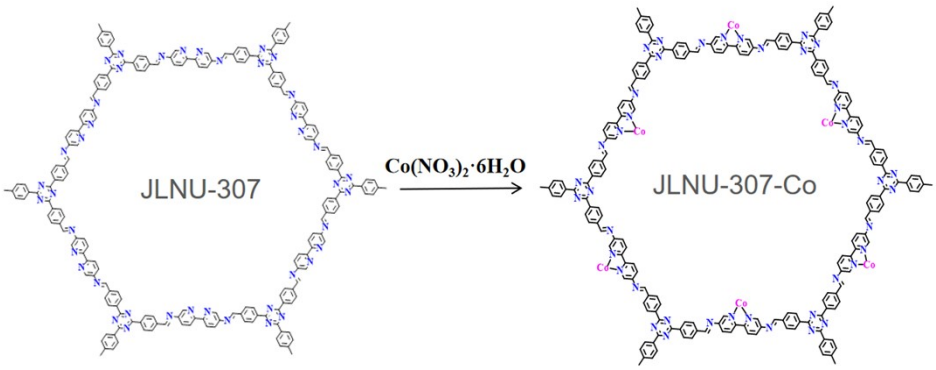

50 mg of JLNU-307 and 100 mg of hexahydrate and cobalt nitrate ($Co(NO_3)_2 \cdot 6H_2O$) were stirred in a mixture of 10 mL of water and ethanol (H_2O:C_2H_5OH=1:1) for 24 h. After vacuum drying at 60℃ for 12 h, 52.84 mg of orange powder was obtained, named as JLNU-307-Co.

S1.4 Computational details

The theoretical calculations were performed via the Gaussian 16 suite of programs [1]. The structure of the studied molecule was fully optimized at the B3LYP-D3BJ/TZVP level of theory. The vibrational frequencies of the optimized structures were carried out at the same level. The structures were characterized as a local energy minimum on the potential energy surface by verifying that all the vibrational frequencies were real. The Hirshfeld atomic charges and the Fukui index (f^+, f^-, f^0) of molecules were calculated and analyzed by using the Multiwfn software [2]. The Visual Molecular Dynamics (VMD) program [3] was used to plot the color-filled iso-surface graphs to visualize the molecular electrostatic potential (MESP). The ESP surface minima and maxima of the molecules are depicted as blue and yellow points, which were calculated based on the optimized structure.

Considering acetonitrile as polar solvent, all structures were optimized and characterized in gas at M06 [4]/BSI level, BSI representing a basis set with SDD [5] for Co and 6-31G(d,p) for other atoms. Harmonic frequency analysis calculations at the same level were performed to verify the optimized geometries to be minima (no imaginary frequency). The energies were further improved by M06/BSII//M06/BSI single-point calculations, BSII denotes a basis set with SDD for Co and 6-311++G(d,p) for other atoms. All DFT calculations were carried

out using Gaussian 09 program [6]. Selected computed structures are illustrated using the CYLview [7].

Section S2: PXRD patterns

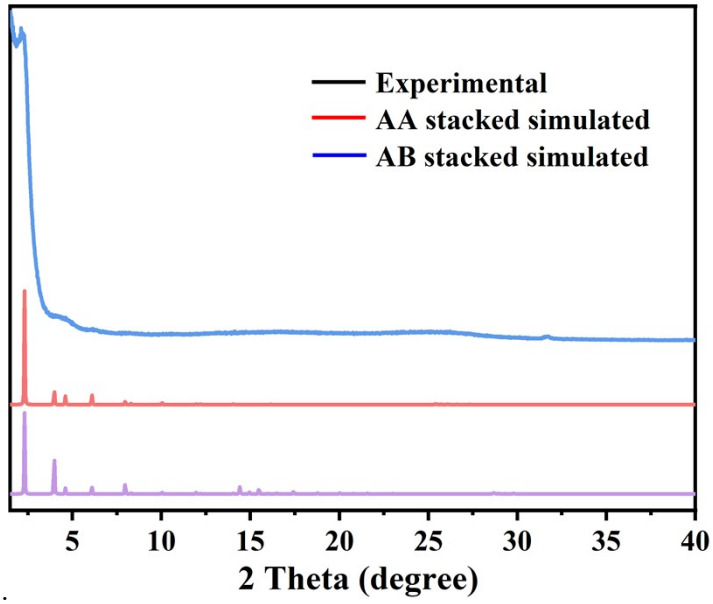

Fig. S1. Comparison of PXRD patterns for JLNU-307: calculated based on the AA stacked (purple), AB stacked (orange), and experiment (blue).

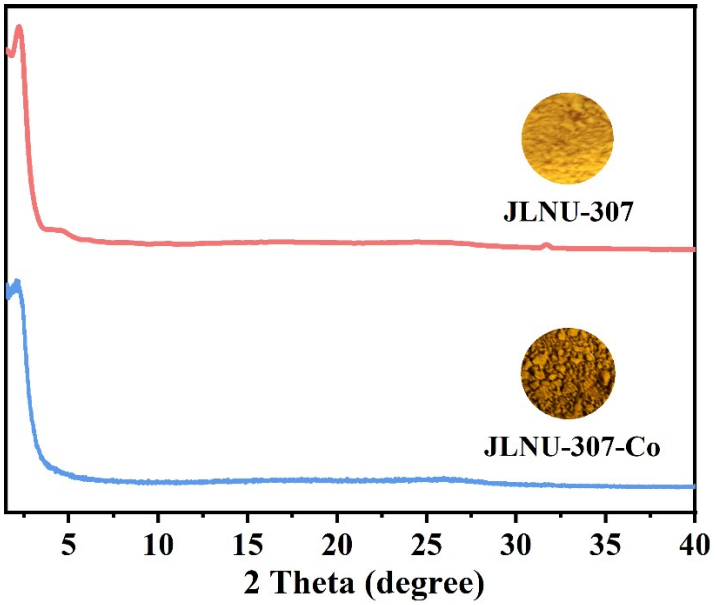

Fig. S2. Comparison of PXRD between JLNU-307 and JLNU-307-Co.

Section S3: Structural model

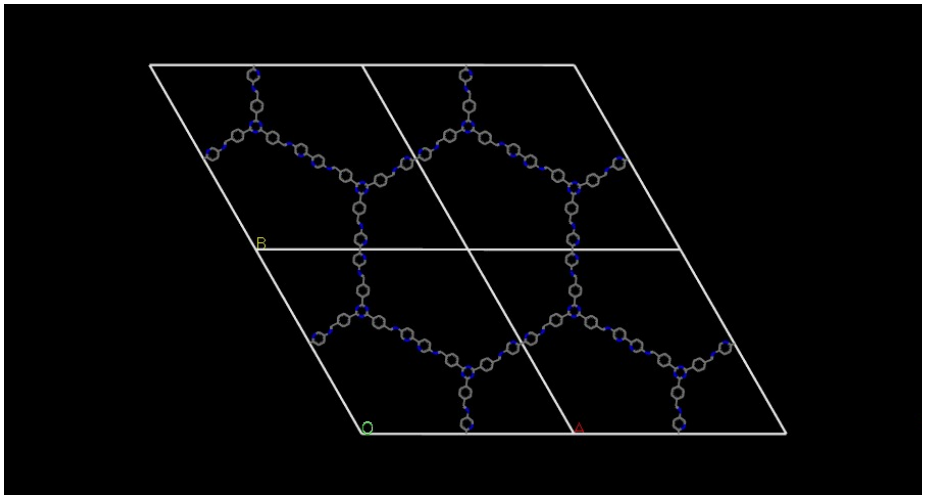

Fig. S3. The simulated AA stacking structure of JLNU-307.

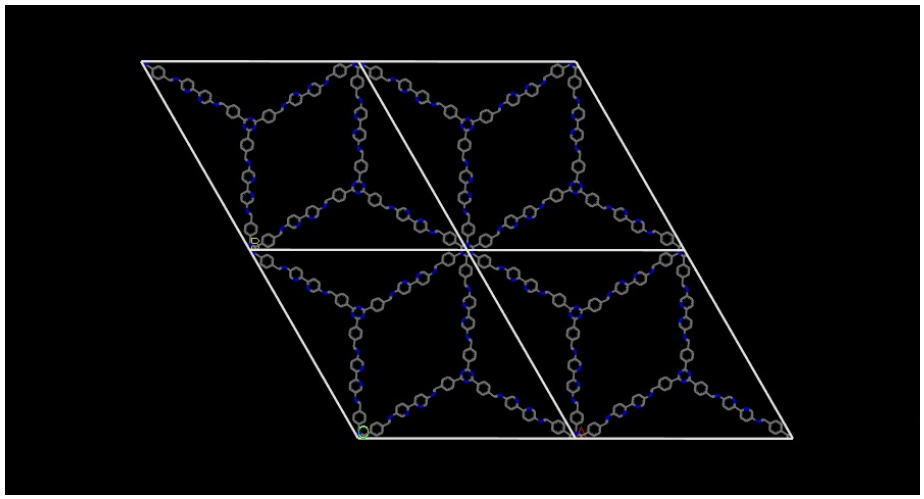

Fig. S4. The simulated AB stacking structure of JLNU-307.

Section S4: Stability test

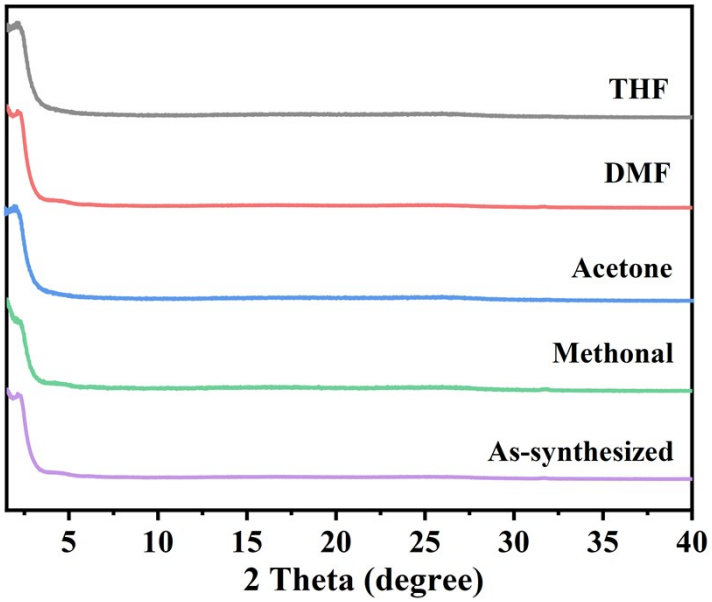

Fig. S5. PXRD patterns of JLNU-307 after 3 d treatment in acid/base aqueous solutions.

Section S5: TGA

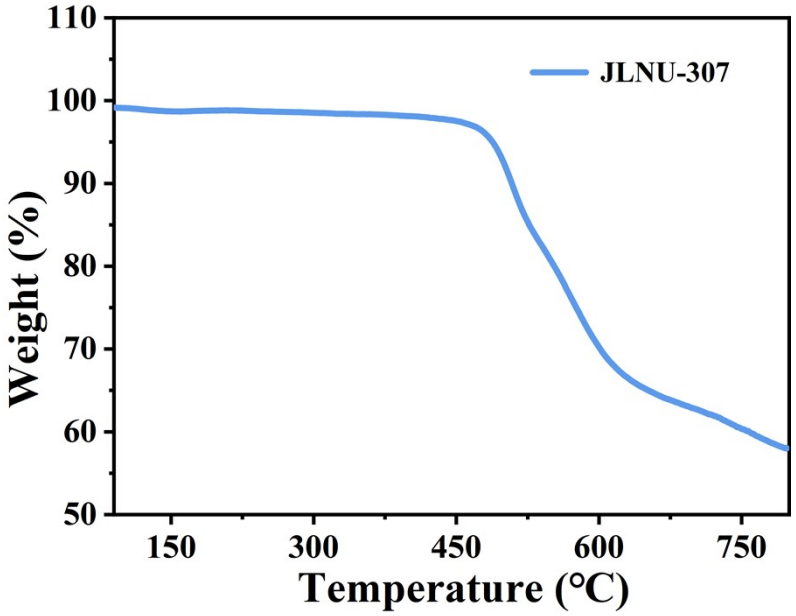

Fig. S6. TGA curves of JLNU-307 in N_2 atmosphere.

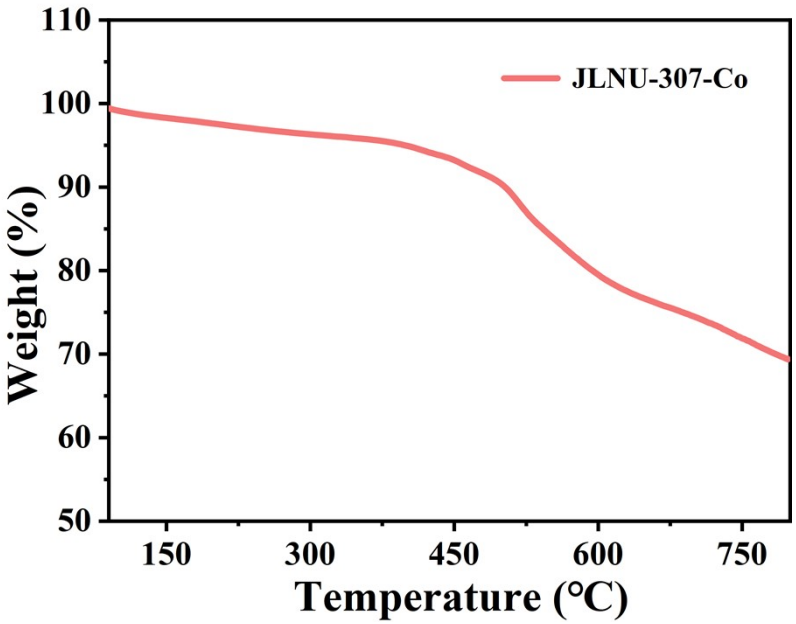

Fig. S7. TGA curves of JLNU-307-Co in N_2 atmosphere.

Section S6: SEM

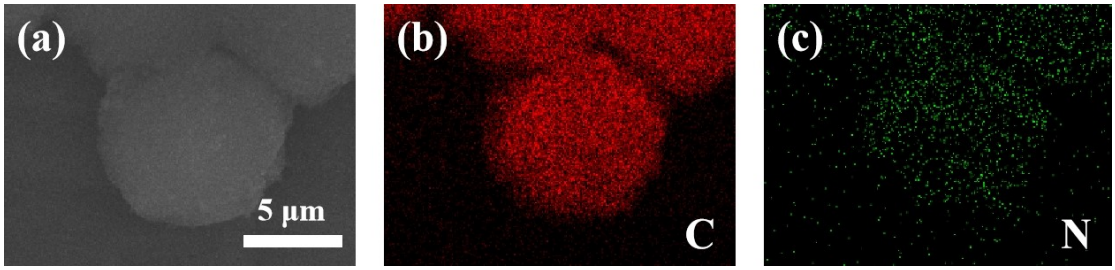

Fig. S8. (a) SEM image of JLNU-307; (b, c) SEM images and EDS maps for C and N elements of JLNU-307.

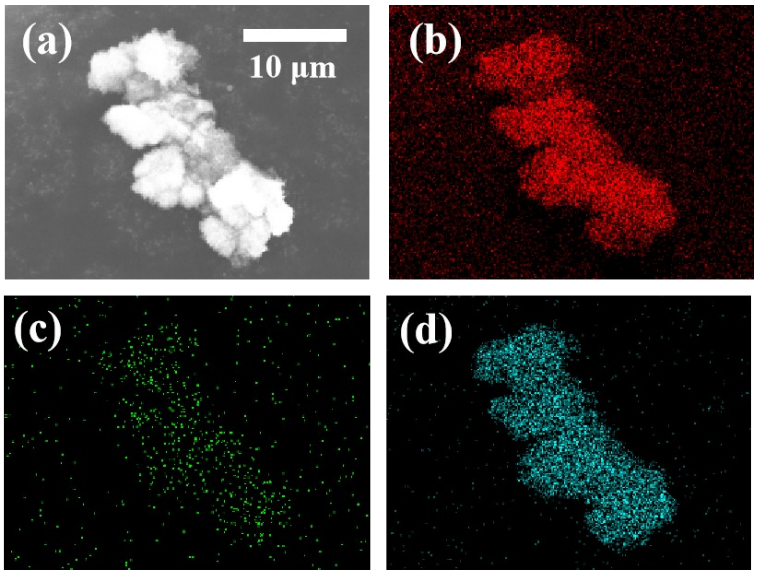

Fig. S9. (a) SEM image of JLNU-307-Co; (b-d) SEM images and EDS maps for C, N and Co elements of JLNU-307-Co.

Section S7: Gas adsorption isotherms

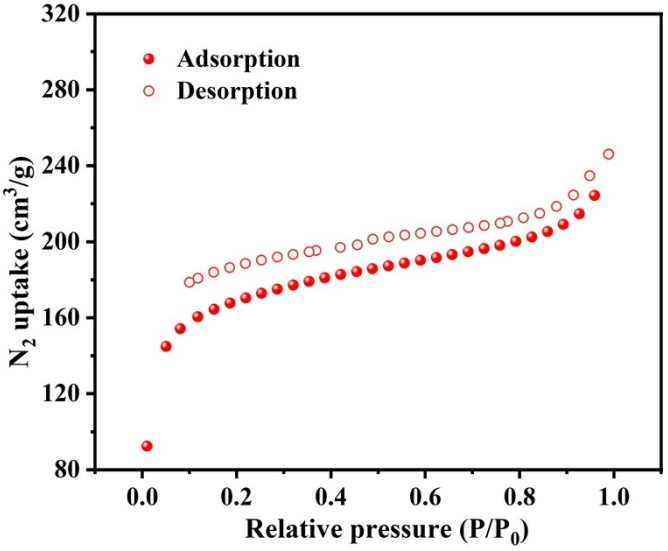

Fig. S10. N_2 adsorption-desorption isotherms of JLNU-307.

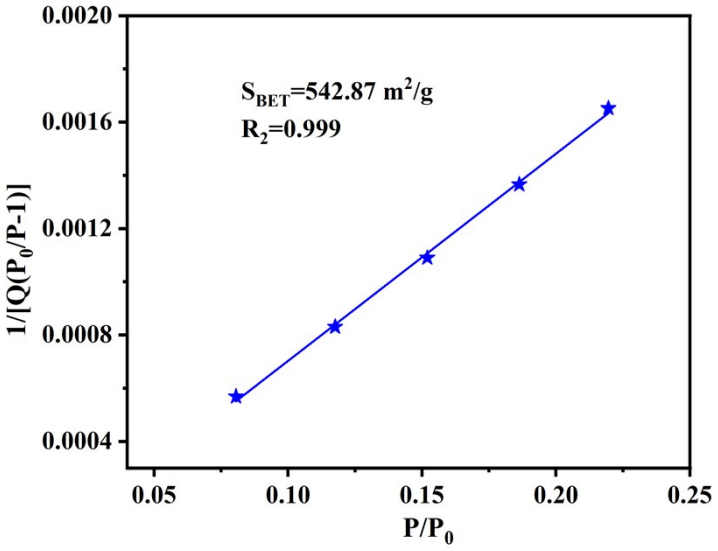

Fig. S11. BET pole of JLNU-307 calculated from N_2 adsorption isotherm at 77 K.

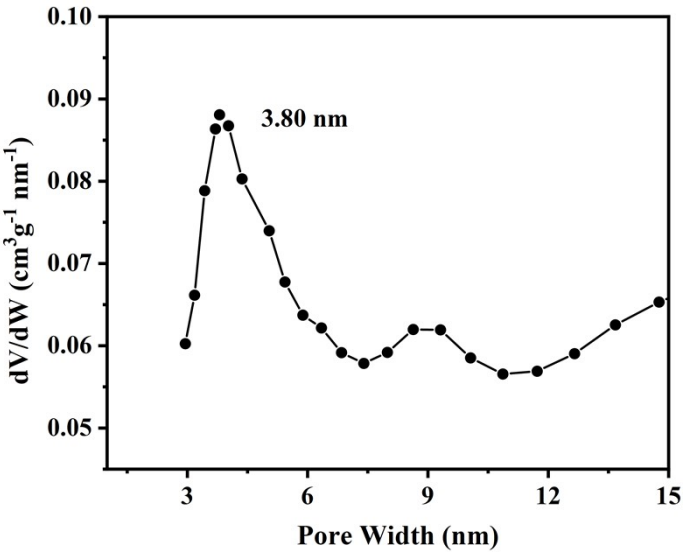

Fig. S12. The pore size distribution curve of JLNU-307.

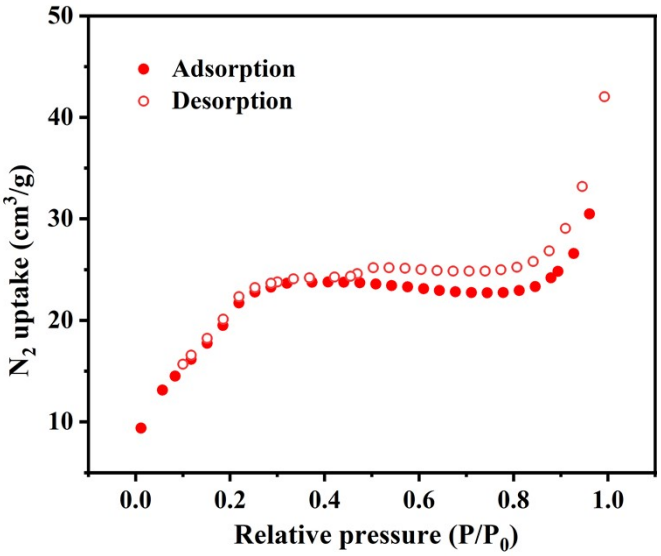

Fig. S13. N_2 adsorption-desorption isotherms of JLNU-307-Co.

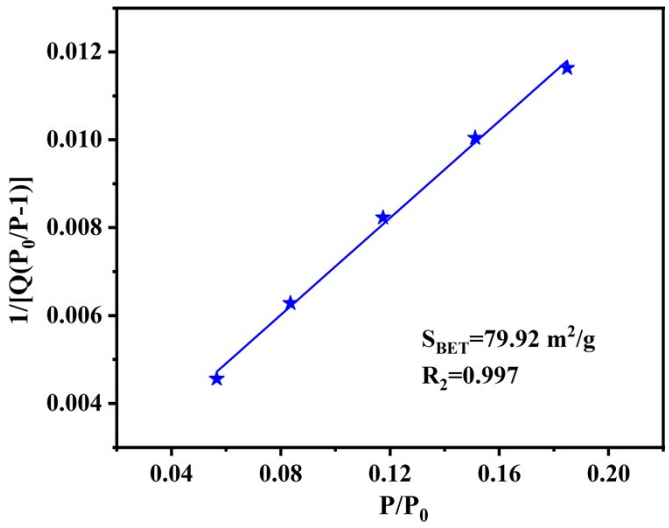

Fig. S14. BET pole of JLNU-305-Co calculated from N_2 adsorption isotherm at 77 K.

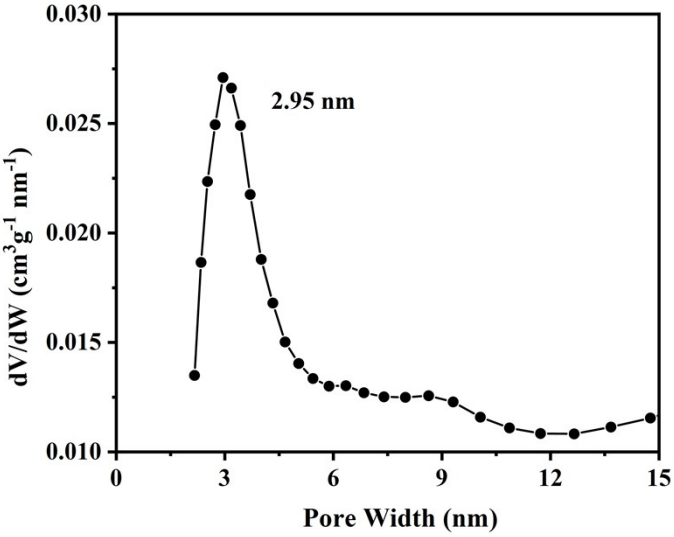

Fig. S15. The pore size distribution curve of JLNU-305-Co.

Section S8: XPS spectra

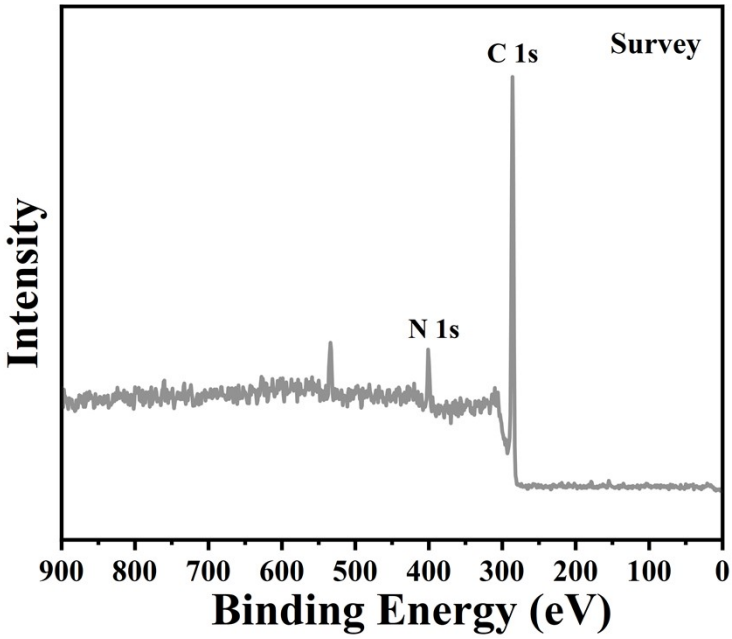

Fig. S16. XPS spectra of JLNU-307.

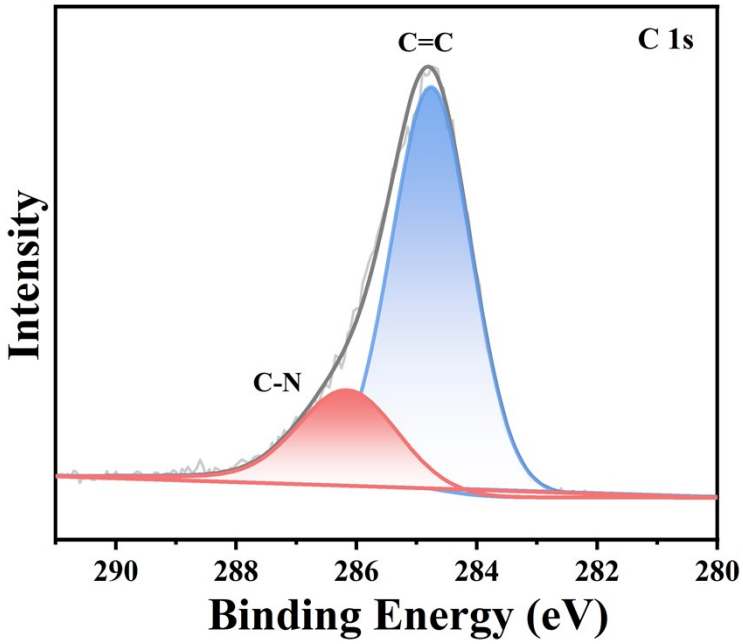

Fig. S17. High resolution XPS spectra of C 1s obtained from JLNU-307.

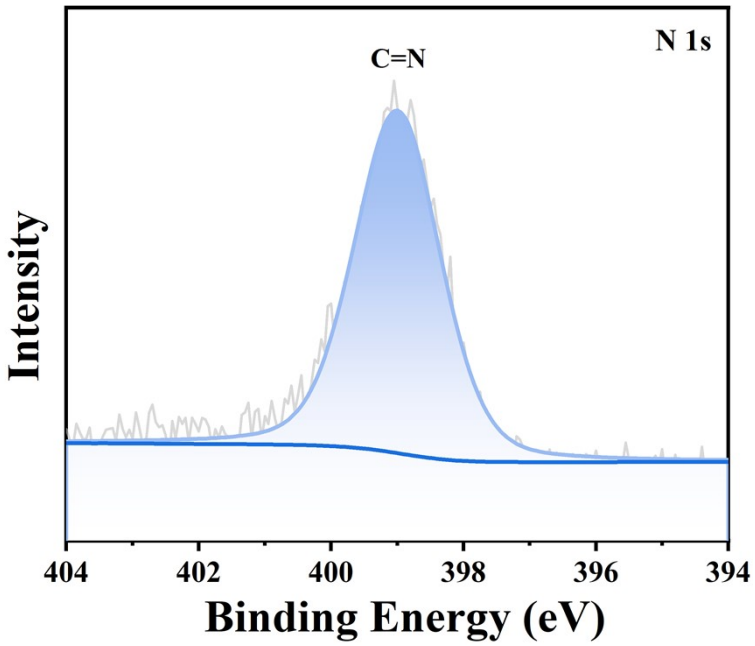

Fig. S18. High resolution XPS spectra of N 1s obtained from JLNU-307.

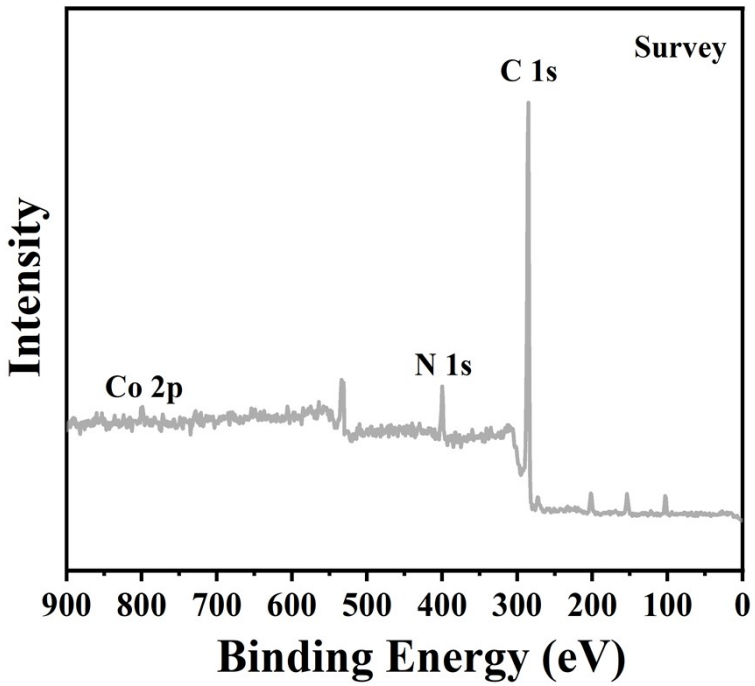

Fig. S19. XPS spectra of JLNU-307-Co.

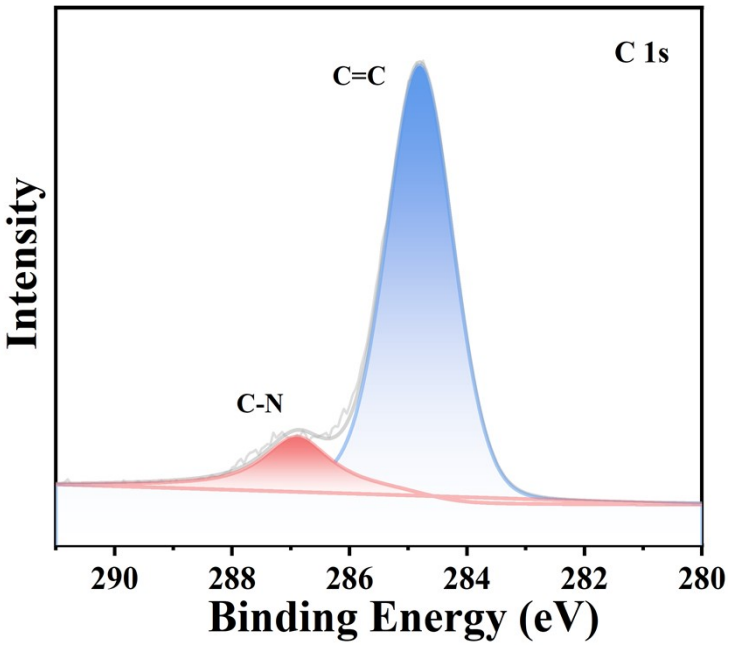

Fig. S20. High resolution XPS spectra of C 1s obtained from JLNU-307-Co.

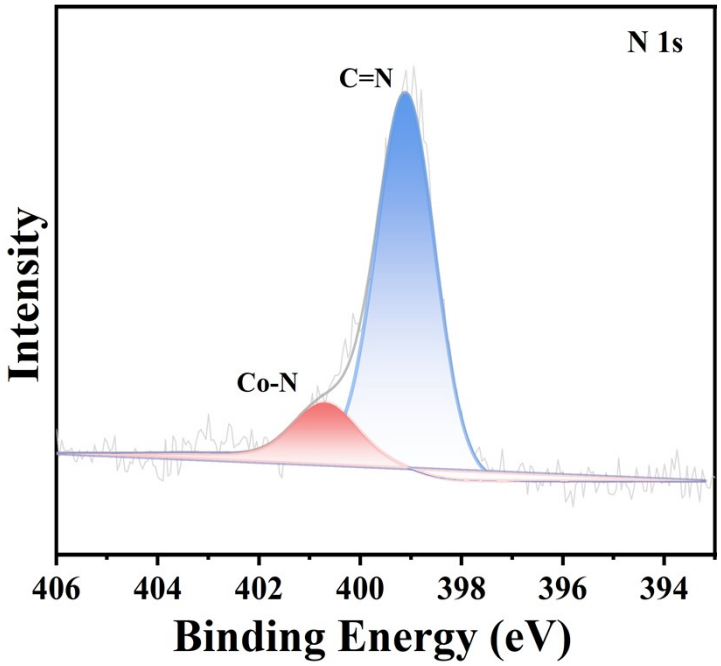

Fig. S21. High resolution XPS spectra of N 1s obtained from JLNU-307-Co.

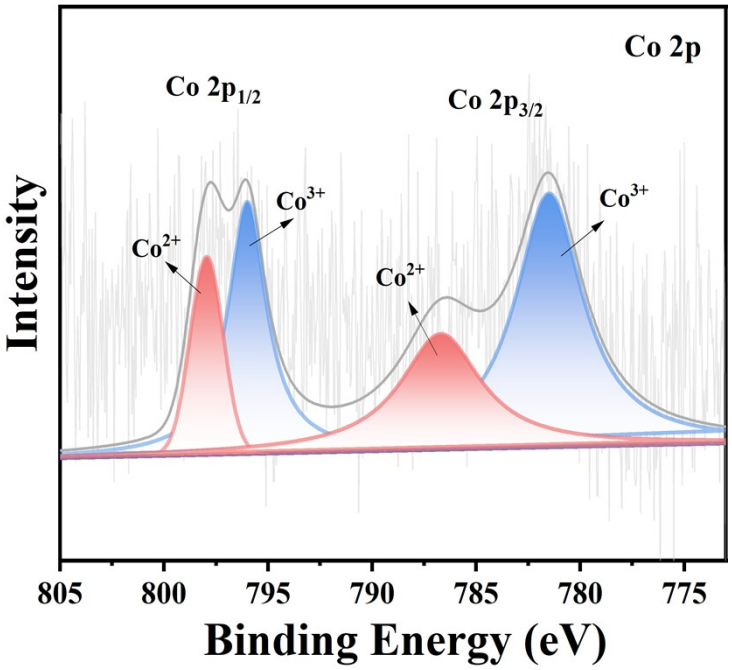

Fig. S22. High resolution XPS spectra of Co 2p obtained from JLNU-307-Co.

Section S9: Contact angle

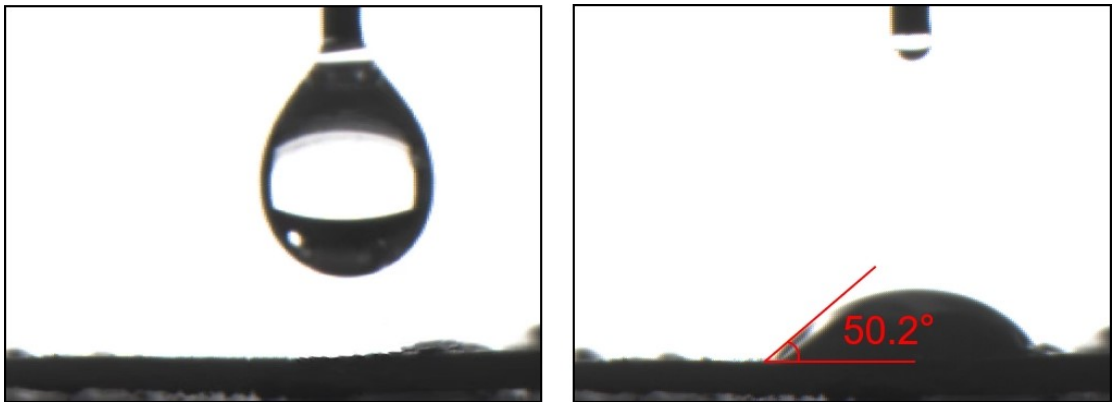

Fig. S23. Contact angle test for JLNU-307.

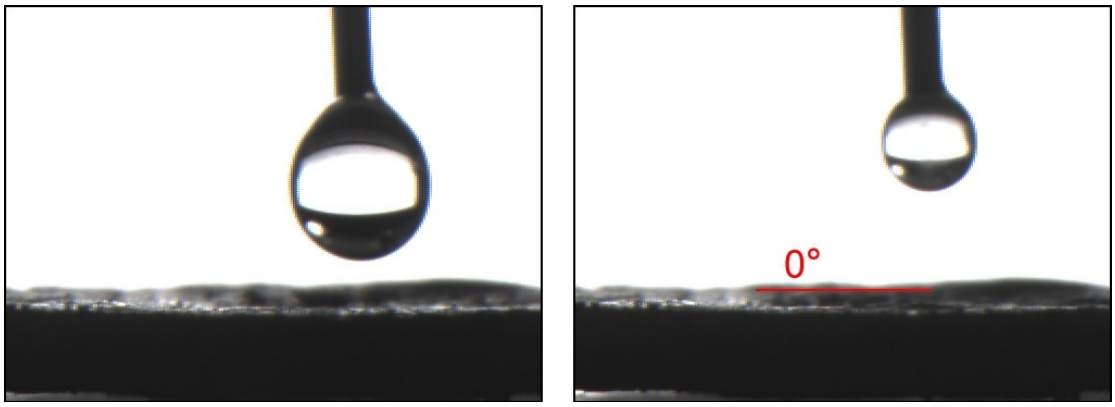

Fig. S24. Contact angle test for JLNU-307-Co.

Section S10: UV-visible absorption

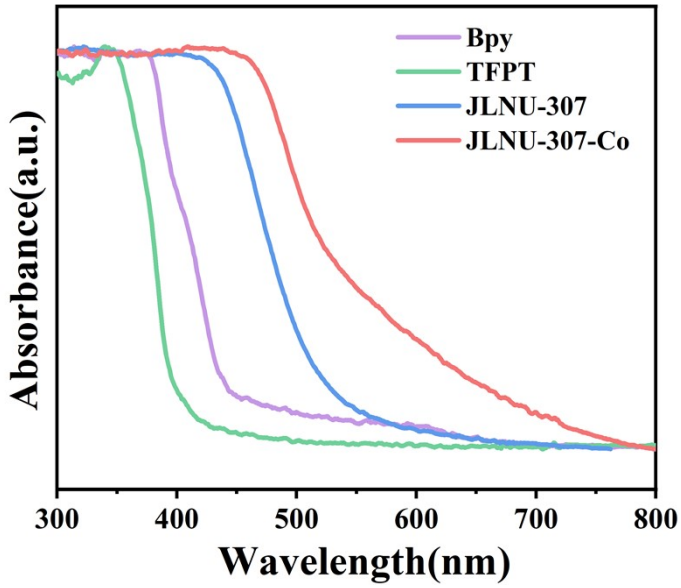

Fig. S25. UV-vis DRS spectra of JLNU-307 and JLNU-307-Co.

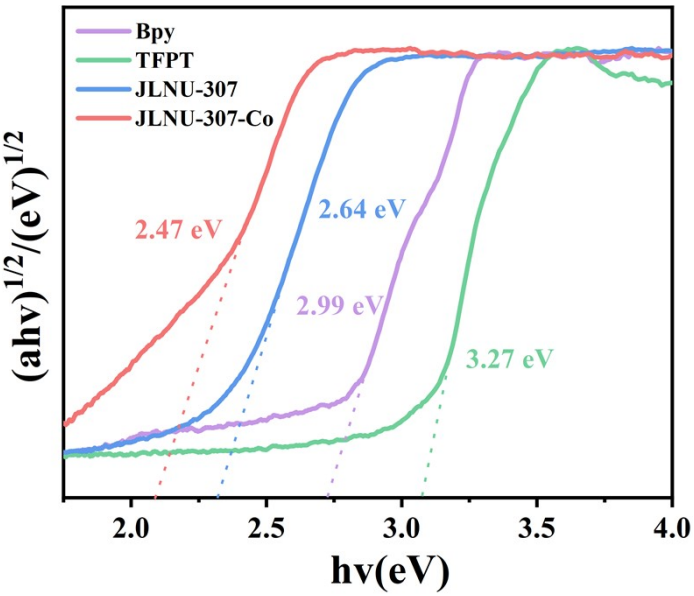

Fig. S26. The bandgap energy of JLNU-307 and JLNU-307-Co.

Section S11: Degradation performance

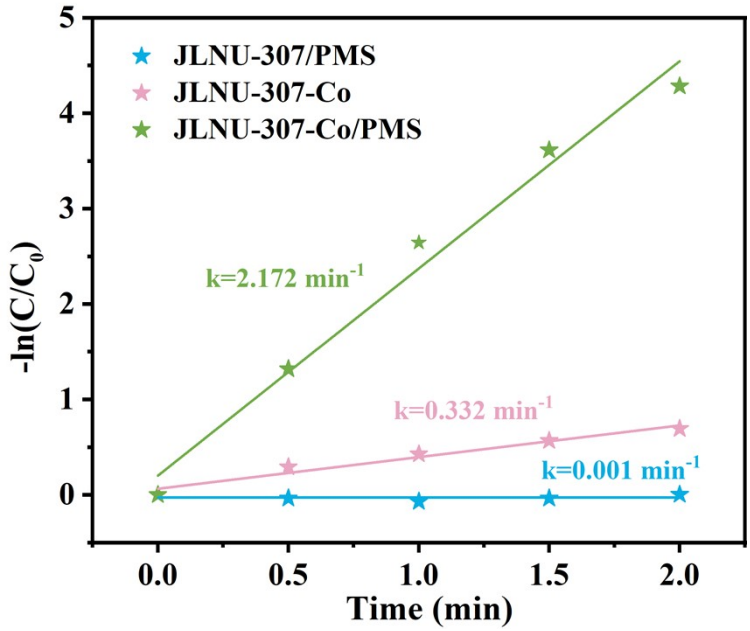

Fig. S27. Reaction rate constants of JLNU-307 and JLNU-307-Co systems within 3 min.

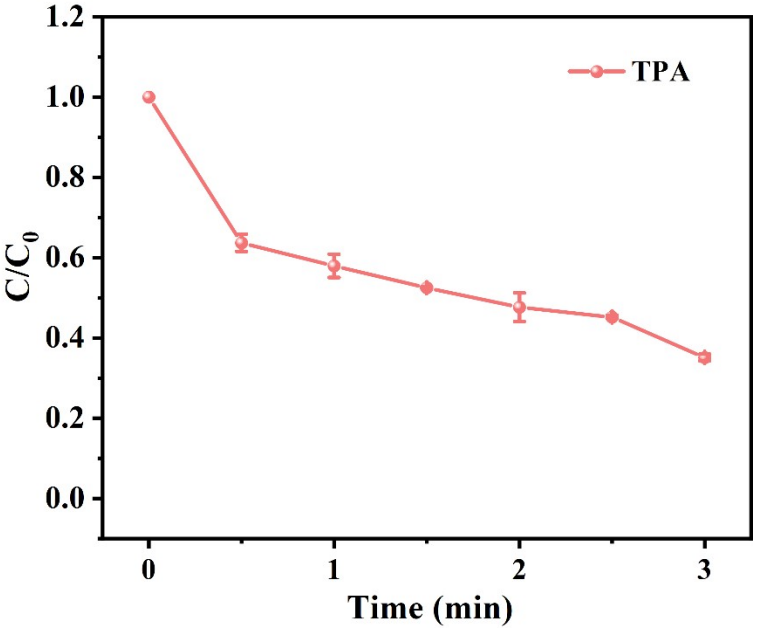

Fig. S28. Effects of TPA (5 mM) on degradation of 2,4-DCP.

Section S12: Unit cell parameters and fractional atomic coordinates

Table S1. Unit cell parameters and fractional atomic coordinates for JLNU-307 calculated on the basis of staggered **hcb** net

Space group		P6/M (No. 175)	
Calculated unit cell		a = b = 44.3729 Å, c = 3.5122 Å, α = β = 90°, γ = 120°	
Measured unit cell		a = b = 44.3729 Å, c = 3.5122 Å, α = β = 90°, γ = 120°	
Pawley refinement		*Rωp* = 2.79%， *Rp* = 1.96%	
Atom	x	y	z
C1	0.50001	0.51926	1
C2	0.51956	0.55571	1
C3	0.50253	0.57495	1
C4	0.46625	0.55796	1
C5	0.44752	0.52147	1
N6	0.46461	0.50319	1
N7	0.44924	0.57815	1
C8	0.41569	0.56435	1
C9	0.39925	0.58593	1
C10	0.36296	0.56972	1
C11	0.34664	0.5897	1
C12	0.36647	0.62614	1
C13	0.40288	0.64231	1
C14	0.4192	0.62234	1
C15	0.34925	0.6472	1
N16	0.31397	0.63147	1
C17	0.48074	0.98075	1
C18	0.44429	0.96385	1
C19	0.42505	0.92758	1
C20	0.44204	0.90829	1
C21	0.47853	0.92605	1
N22	0.49681	0.96142	1
N23	0.42185	0.87109	1

Section S13: Compared with other catalysts

Table S2. Comparison of the performance of JLNU-305-Fe with other catalysts.

Catalyst	Pollutants:2,4-DCP					Reference
	Amount of catalyst (mg)	Concentration of pollutants (mg/L)	Time of degradation (min)	Illumination	Efficiency of degradation (%)	
JLNU-307-Co/PMS	10	50	3	—	100	**This work**
Pal-Fe/Ni	75	81.5	240	—	100	8
GCN-PSFs	25	5	30	√	88.8	9
Cr(VI)/PCN-S	50	80	80	√	100	10
1Ag/6Sn-CN	200	20	30	—	71	11
$Na_{(8)}B_{(6)}$-CN	50	50	270	√	90.6	12

Fe/Mn-BC/PS	100	30	30	—	83.7	13
MIL-100(Fe)	75	100	420	√	87.7	14
D-ATP-nFe/Ni	400	10	120	—	96.8	15
Fe@C/Cu@C-PS	94	40	90	—	100	16
COFs-Ph@CdS-3	20	10	100	√	95.4	17
Fe_3O_4(S600)/PMS	200	20	70	√	100	18
JLNU-305-Fe/PDS	10	10	8	—	100	19
CoNi LDH@NF/PMS	200	20	90	—	99	20
$FeCo_2O_4$/PMS	60	100	90	—	95	21

Section S14. References

[1] M. J. Frisch, G. W. Trucks, H. B. Schlegel, et al., Gaussian 16 Revision. A.03, Gaussian Inc., Wallingford, CT, 2016.

[2] Lu, T. & Chen, F. Multiwfn: a multifunctional wavefunction analyzer. J. Comput. Chem., 33 (2012) 580-592. https://doi.org/10.1002/jcc.22885.

[3] W. Humphrey, A. Dalke and K. Schulten, VMD: Visual molecular dynamics. J Mol Graph Model, (1996) 14, 33-38. https://doi.org/10.1016/0263-7855(96)00018-5.

[4] (a) Y. Zhao, D. G. Truhlar, J. Chem. Theory Comput. 2009, 5, 324; (b) Y. Zhao, D. G. Truhlar, Theor. Chem. Acc. 2008, 120, 215; (c) Y. Zhao, D. G. Truhlar, Acc. Chem. Res. 2008, 41, 157.

[5] (a) M. Dolg, U. Wedig, H. Stoll, H. Preuss, J. Chem. Phys. 1987, 86, 866; (b) D. Andrae, U. Häussermann, M. Dolg, H. Stoll, H. Preuss, Theor. Chim. Acta. 1990, 77, 123; (c) L. E. Roy, P. J. Hay, R. L. Martin, J. Chem. Theory. Comput. 2008, 4, 1029.

[6] (a) Y. Zhao, D. G. Truhlar, J. Chem. Theory Comput. 2009, 5, 324; (b) Y. Zhao, D. G. Truhlar, Theor. Chem. Acc. 2008, 120, 215; (c) Y. Zhao, D. G. Truhlar, Acc. Chem. Res. 2008, 41, 157. 6 M. J. Frisch, G. W. Trucks, H. B. Schlegel, G. E. Scuseria, M. A. Robb, J. R. Cheeseman, G. Scalmani, V. Barone, B. Mennucci, G. A. Petersson, H. Nakatsuji, M. Caricato, X. Li, H. P. Hratchian, A. F. Izmaylov, J. Bloino, G. Zheng, J. L. Sonnenberg, M. Hada, M. Ehara, K. Toyota, R. Fukuda, J. Hasegawa, , M. Ishida, T.Nakajima, Y. Honda, O. Kitao, H. Nakai, T. Vreven, J. A. Montgomery, Jr.; J. E. Peralta, F. Ogliaro, M. Bearpark, J. J. Heyd, E. Brothers, K. N. Kudin, V. N. Staroverov, T. Keith, R. Kobayashi, J. Normand, K. Raghavachari, A. Rendell, J. C. Burant, S. S. Iyengar, J. Tomasi, M. Cossi, N. Rega, J. M. Millam, M. Klene, J. E. Knox, J. B. Cross, V. Bakken, C. Adamo, J. Jaramillo, R. Gomperts, R. E. Stratmann, O. Yazyev, A. J. Austin, R. Cammi, C. Pomelli, J. W. Ochterski, R. L. Martin, K. Morokuma, V. G. Zakrzewski, G. A. Voth, P. Salvador, J. J. Dannenberg, S. Dapprich, A. D. Daniels, O. Farkas, J. B. Foresman, J. V. Ortiz, J. Cioslowski, and D. J. Fox, Gaussian 09, Rev. A.01; Gaussian, Inc.: Wallingford, CT, 2010.

[7] C. Y. Legault, CYLView, version 1.0 b; Université de Sherbrooke: Sherbrooke, Quebec, Canada, 2009. http://www.cylview.org.

[8] N. Ezzatahmadi, G.J. Millar, G.A. Ayoko, J. Zhu, R. Zhu, X. Liang, H. He, Y. Xi, Degradation of 2,4-dichlorophenol using palygorskite-supported bimetallic Fe/Ni nanocomposite as a heterogeneous catalyst, Appl Clay Sci. 168 (2019) 276-286. https://doi.org/10.1016/j.clay.2018.11.030.

[9] Y. Wu, J. Chen, H. Che, X. Gao, Y. Ao, P. Wang, Boosting $2e^-$ oxygen reduction reaction in garland carbon nitride with carbon defects for high-efficient photocatalysis-self-Fenton degradation of 2,4-dichlorophenol, Appl. Catal. B. 307 (2022) 121185. https://doi.org/10.1016/j.apcatb.2022.121185.

[10] Y. Deng, L. Tang, G. Zeng, Z. Zhu, M. Yan, Y. Zhou, J. Wang, Y. Liu, J. Wang, Insight into highly efficient simultaneous photocatalytic removal of Cr(VI) and 2,4-diclorophenol under visible light irradiation by phosphorus doped porous ultrathin g-C_3N_4 nanosheets from aqueous media: Performance and reaction mechanism, Appl. Catal. B. 203 (2017) 343-354. https://doi.org/10.1016/j.apcatb.2016.10.046.

[11] W. Ali, X. Zhang, X. Zhang, S. Ali, L. Zhao, S. Shaheen, L. Jing, Improved visible-light activities of g-C_3N_4 nanosheets by co-modifying nano-sized SnO_2 and Ag for CO_2 reduction and 2,4-

dichlorophenol degradation, Mater. Res. Bull. 122 (2020) 110676. https://doi.org/10.1016/j.materresbull.2019.110676.

[12] Y. Chu, X. Zheng, J. Fan, Preparation of sodium and boron co-doped graphitic carbon nitride for the enhanced production of H_2O_2 via two-electron oxygen reduction and the degradation of 2,4-DCP via photocatalytic oxidation coupled with Fenton oxidation, Chem. Eng. J. 431 (2022) 134020. https://doi.org/10.1016/j.cej.2021.134020.

[13] K. Zhang, D. Huang, Y. Zhang, N. El Houda Bouroubi, P. Chen, N. Ganbold, P. He, J. Liu, Y. Fang, M. Gan, J. Zhu, B. Yang, Natural mineral-derived Fe/Mn-BC as efficient peroxydisulfate activator for 2,4-dichlorophenol removal from wastewater: Performance and sustainable catalytic mechanism, J. Environ. Manage. 335 (2023) 117540. https://doi.org/10.1016/j.jenvman.2023.117540.

[14] Z. Wang, R. Miao, L. He, Q. Guan, Y. Shi, Green synthesis of MIL-100(Fe) derivatives and revealing their structure-activity relationship for 2,4-dichlorophenol photodegradation, Chemosphere. 291 (2022) 132950. https://doi.org/10.1016/j.chemosphere.2021.132950.

[15] H. Wu, J. Wang, H. Liu, X. Fan, Performance, Reaction Pathway and Kinetics of the Enhanced Dechlorination Degradation of 2,4-Dichlorophenol by Fe/Ni Nanoparticles Supported on Attapulgite Disaggregated by a Ball Milling-Freezing Process, Materials, 15 (2022) 3957. https://doi.org/10.3390/ma15113957.

[16] S. Zhou, Y. Hu, M. Yang, Y. Liu, Q. Li, Y. Wang, G. Gu, M. Gan, Insights into the mechanism of persulfate activation with carbonated waste metal adsorbed resin for the degradation of 2,4-dichlorophenol, Environ. Res. 226 (2023) 115639. https://doi.org/10.1016/j.envres.2023.115639.

[17] D. You, Z. Pan, Q. Cheng, COFs-Ph@CdS S-scheme heterojunctions with photocatalytic hydrogen evolution and efficient degradation properties, J. Alloys Compd. 930 (2023) 167069. https://doi.org/10.1016/j.jallcom.2022.167069.

[18] Wang, H., Liu, H., Chu, Z., Sun, F., Zou, X., Wang, Q., Wang, H. Fe_3O_4 Derived from the Decomposition of Siderite as a Heterogeneous Photocatalyst to Degrade 2,4-DCP Via Activating PMS: The Enhancement of Visible Light Irradiation. J. Water Process Eng

,(2024) 4524012. https://doi.org/10.1016/j.jwpe.2023.104538

[19] Y. Han, M. Tai, Y. Yao, J. Li, Y. Wu, B. Hu, Y. Ma, C. Liu, Iron-decorated covalent organic framework as efficient catalyst for activating peroxydisulfate to degrade 2,4-dichlorophenol: Performance and mechanism insight, J. Colloid Interface Sci, 663 (2024) 238-250. https://doi.org/10.1016/j.jcis.2024.02.165.

[20] Liu, Y., Liu, W., Gan, X., Shang, J., & Cheng, X. High-performance, stable CoNi LDH@ Ni foam composite membrane with innovative peroxymonosulfate activation for 2,4-dichlorophenol destruction. J. Environ. Sci, 141 (2024) 235-248. https://doi.org/10.1016/j.jes.2023.07.019.

[21] Zhou, R., Zhao, J., Shen, N., Ma, T., Su, Y., Ren, H. Efficient degradation of 2,4-dichlorophenol in aqueous solution by peroxymonosulfate activated with magnetic spinel FeCo2O4 nanoparticles. Chemosphere, 197 (2018) 670-679. https://doi.org/10.1016/j.chemosphere.2018.01.079.